

**Title: Rapid in situ assessment of radiocesium wood contamination using field gamma-ray spectroscopy to optimise felling.**

Authors: Adam Varley<sup>1</sup>, Andrew Tyler<sup>1</sup>, Maksim Kudzin<sup>3</sup>, Viachaslau Zabrotski<sup>3</sup>, Justin Brown<sup>2</sup>, Taras Bobrovskiy<sup>2</sup> and Mark Dowdall<sup>2</sup>.

**Affiliations:**

<sup>1</sup>Department of Biological and Environmental Sciences, University of Stirling, Stirling FK9 4LA, United Kingdom

<sup>2</sup>Norwegian Radiation Protection Authority, Grini næringspark 13, 1332 Østerås, Norway

<sup>3</sup>Polessie State Radiation-Ecological Reserve, Tereshkovoy Street 7, Khoyniki, Gomel Region, Belarus

Corresponding author's email address: [a.l.varley@stir.ac.uk](mailto:a.l.varley@stir.ac.uk)

Accepted refereed manuscript of:

Varley A, Tyler A, Kudzin M, Zabrotski V, Brown J, Bobrovskiy T & Dowdall M (2020) Rapid in situ assessment of radiocesium wood contamination using field gamma-ray spectroscopy to optimise felling. *Journal of Environmental Radioactivity*, 218, Art. No.: 106259. DOI:

<https://doi.org/10.1016/j.jenvrad.2020.106259>

© 2020, Elsevier. Licensed under the Creative Commons Attribution-NonCommercial-NoDerivatives 4.0 International <http://creativecommons.org/licenses/by-nc-nd/4.0/>

## Highlights:

- Characterising caesium contamination in wood is one of the principal issues
- Current methods are inefficient leading to large volumes of waste.
- In situ and mobile gamma-ray spectrometry offer a means of real-time characterisation

## Abstract

The Chernobyl nuclear power meltdown that took place in 1986 has left a radioactive contamination legacy that currently severely limits the economic potential of impacted regions including the Polessie State Radioecology Reserve in Southern Belarus. Extensive areas of forested land could potentially become economically viable for firewood and building materials if radioactive contamination, notably  $^{137}\text{Cs}$ , could be characterised faster, whilst closely adhering to regulatory limits. Currently, laboursome tree coring and unreliable transfer factors derived from limited soil sampling data are routinely employed in felling decision making, which has financial repercussions owed to the large amounts of waste produced and unnecessary transportation costs. In this study, it is demonstrated that a combination of targeted mobile gamma-ray spectrometry and a newly developed, lead shielded, *in situ* gamma-ray spectrometry method can significantly speed up the process of characterisation of  $^{137}\text{Cs}$  wood activity in the field. For the *in situ* method, Monte Carlo calibration routines were developed alongside spectral processing procedures to unfold spectra collected in the field allowing for separation of ground and tree spectral components. Isolated contributions from the tree could then be converted to activity. The method was validated at a test facility and then demonstrated at three separate sites with differing contamination levels. This technique showed that single trees could be measured within approximately 20 % of the activity compared to conventional tree core data. However, some discrepancies were found which were attributed to under sampling using the tree corer and low count rates at the lowest activity site, prompting the need for further data collection to optimise the method. It was concluded that this real-time approach could be a valuable tool for management of contaminated forested areas, releasing valuable timber and ultimately reducing the risk associated with living and working in these areas.

## 1 **1. Introduction**

2 The Chernobyl accident of April 1986 resulted in the world's largest nuclear disaster, wide  
3 scale radioactive contamination being spread over much of Northern Europe with the highest  
4 deposition of contamination occurring over large areas of the former USSR countries  
5 encompassing modern day Russia, Belarus and Ukraine (IAEA, 2008). Areas in close  
6 proximity of the nuclear power plant were particularly impacted leading to evacuation. Large  
7 tracts of forested land exist in these regions which are intrinsically linked to efforts towards  
8 socio-economic revitalisation of the impacted areas. The most contaminated regions in Belarus  
9 occur in the southern reaches of the Gomel Region, along the border with the Ukraine. The  
10 Belarusian exclusion zone functions as a scientific reserve, the Polessie State Radiation-  
11 Ecological Reserve (PSRER), which covers some 216 thousand hectares. The PSRER is  
12 located in a subzone of foliar (deciduous and broad-leaved) and pine woods, with forested areas  
13 constituting 109.7 thousand hectares (51.1 % of the territory). Pine woods comprise 43.9 % of  
14 the afforested areas, birch woods 30.7 %, black alder 12.4 %, oak 6.3 % and other species 6.7  
15 %. The territories not covered by forest (primarily abandoned agricultural lands) are 82.2  
16 thousand hectares (38.0 %) and non-agricultural unforested lands occupy 20.1 thousand  
17 hectares (9.3 %) (Izrael et al., 1996).

18

19 Until recent years, the management of Chernobyl contaminated land, inclusive of the PSRER,  
20 has been primarily oriented towards reducing external and internal doses to the public and  
21 mitigating the risks for further dispersal of contaminants through natural events such as  
22 forestfires or wildfires (Dvornik et al., 2018; Evangelidou, 2015). Irrespective of the radiological  
23 challenges posed by contamination for forestry workers or residents of forested areas, there are  
24 still direct and indirect economic impacts imposed due to radioactive contamination of forests  
25 (Yoshihara et al., 2014). This is primarily in relation to regulatory limits imposed on wood and  
26 wood products and their effects on the development of forestry resources (Shaw et al., 2001).  
27 The important role of forestry and derived products in the current and future Belarusian  
28 economy is well established (Gerasimov and Karjalainen, 2010). The area of Belarus with the  
29 most forest coverage is the Gomel region and some 2 million ha (21 % of the forest fund area)  
30 continues to be impacted by contamination derived from Chernobyl (Woodfuels Program,  
31 2009). Wood harvesting is prohibited in areas with contamination densities in excess of 1.4  
32 MBq m<sup>-2</sup>. Relevant regulatory limits for Belarus are displayed in Table 1.

33

34 Table 1. National admissible levels for the  $^{137}\text{Cs}$  content of timber, timber goods and other  
 35 non-food forestry products in Belarus (RDU/LH-2001, 2001)

Product/Material	$^{137}\text{Cs}$ , Bq/kg
Roundwood for construction of the walls of residential housing	740
Other roundwood products	1480
Process wood	1480
Fuel wood	740
Lumber, wooden goods and construction components (internal) for residential housing	740
Lumber, wooden goods and components, other	1850
Other inedible products	1850

36

37 Until recently, the assessment of  $^{137}\text{Cs}$  content in contaminated forest stands has largely been  
 38 based on transfer factors (TF;  $\text{Bq kg}^{-1}/\text{Bq m}^{-2}$ ) that are based on comparing the  $^{137}\text{Cs}$   
 39 concentration in a given tree component ( $\text{Bq kg}^{-1}$ ) to the total  $^{137}\text{Cs}$  contamination density of  
 40 the soil ( $\text{Bq m}^{-2}$ ) (Nimis, 1996). Many TF models have been developed using various different  
 41 radionuclide, tree and soil types and have been widely used to assess the redistribution of  $^{137}\text{Cs}$   
 42 in forest ecosystems (Ipatyev et al., 1999) and to develop broad-scale maps of forest  
 43 contamination from  $^{137}\text{Cs}$  deposition inventories (Goor and Avila, 2003; van der Perk et al.,  
 44 2004). In terms of building up a general picture of wood activity across a region, TF are a  
 45 practical solution given that they can be derived within a relatively short time frame either  
 46 through direct soil sampling or using pre-existing decay-corrected soil activity data, combined  
 47 with soil composition and land cover maps. However, predictions on a smaller scale, which  
 48 are more relevant to the forestry industry, such as over tens of meters, are far more difficult  
 49 owing to the environment being innately heterogeneous in terms of soil, tree type and  
 50 contamination distribution. Small scale variation in contamination distribution is particularly  
 51 important, as more recent studies have demonstrated that orders of magnitude of change can  
 52 be observed in areas closer to the Chernobyl nuclear power plant (Golosov, 2003; Golosov et  
 53 al., 2000; Adam Varley et al., 2017; Vitaly et al., 2019, 2018). In part this variation is due to

54 remobilisation, but mainly it is down to finer scale deposition patterns dictated by localised  
55 meteorological events in 1986 (Varley et al., 2018). Therefore, basing wood activities for an  
56 entire forest stand from TR derived from limited soil samples leaves a study particularly  
57 vulnerable to very large uncertainties on final estimates.

58 The social and economic role of forestry and its products and potential future commercial  
59 development of contaminated forestry areas necessitates a means of reliably and efficiently  
60 assessing the  $^{137}\text{Cs}$  content of trees. Sampling of trees by coring followed by laboratory analysis  
61 is inefficient due to the number of trees involved and the time and resources required for  
62 sampling and analysis prior to felling. Similarly, alternative methods based on TF's operated  
63 over large areas can be unreliable potentially misclassifying large areas of otherwise productive  
64 forest stand whilst still requiring analysis of potentially unrepresentative soil samples.

65 The ability to reliably estimate the  $^{137}\text{Cs}$  level in the wood of a tree, in real-time, without the  
66 need to fell a tree provides a potentially valuable tool for the forestry industry in areas that are  
67 affected by radioactive contamination. Such a tool would significantly reduce waste as trees  
68 can be screened prior to felling to ensure compliance with regulatory limits and harvesting  
69 effort and resources can be more efficiently applied. In this context, the in situ measurement of  
70  $^{137}\text{Cs}$  in standing trees may offer potential benefits.

### 71 *1.1. Field gamma-ray spectrometry of $^{137}\text{Cs}$*

72 Conventionally, in situ measurements serve to establish the  $^{137}\text{Cs}$  activity deposition ( $\text{Bq m}^{-2}$ )  
73 in the underlying soil and utilise the number of counts in the photopeak at 662 keV (Tyler,  
74 2008). Signal contributions from other environmental media, for example trees, are typically  
75 assumed to be negligible or constant, although attempts have been made at characterising  
76 contributions from tree trunks and the canopy (Cresswell et al., 2016; Gering et al., 2002). For  
77 measurements of the soil activity, a single measurement can be made to derive spatially  
78 integrated activity estimates with appropriate correction, from soil core data or estimated from  
79 inherent spectral features such as the peak-to-valley ratio (Östlund et al., 2015), for vertical  
80 depth distribution of  $^{137}\text{Cs}$  (Miller et al., 1990).

81 However, the use of in situ gamma spectrometry cannot be applied in determining the activity  
82 present in a tree by simply placing a detector against the tree as there are almost always two  
83 significant signal components: (i) from the contaminants in the tree; and (ii) from the

84 contaminants in ground. Untangling the signal is unfeasible as contributions from both (i) and  
85 (ii) can change significantly on both spatial and temporal scales depending on the amount of  
86  $^{137}\text{Cs}$  originally deposited, the properties of the soil and the age and species of the tree (Fogh  
87 and Andersson, 2001). In addition, the primary component of the gamma photon signal in the  
88 detector would be nuisance signal from the ground as the volume of soil within the field of  
89 view of the detector is much larger compared to volume of the tree within the same field of  
90 view (Gering et al., 2002). Furthermore, activities in the ground are orders of magnitude higher  
91 due to low uptake by the tree from the ground.

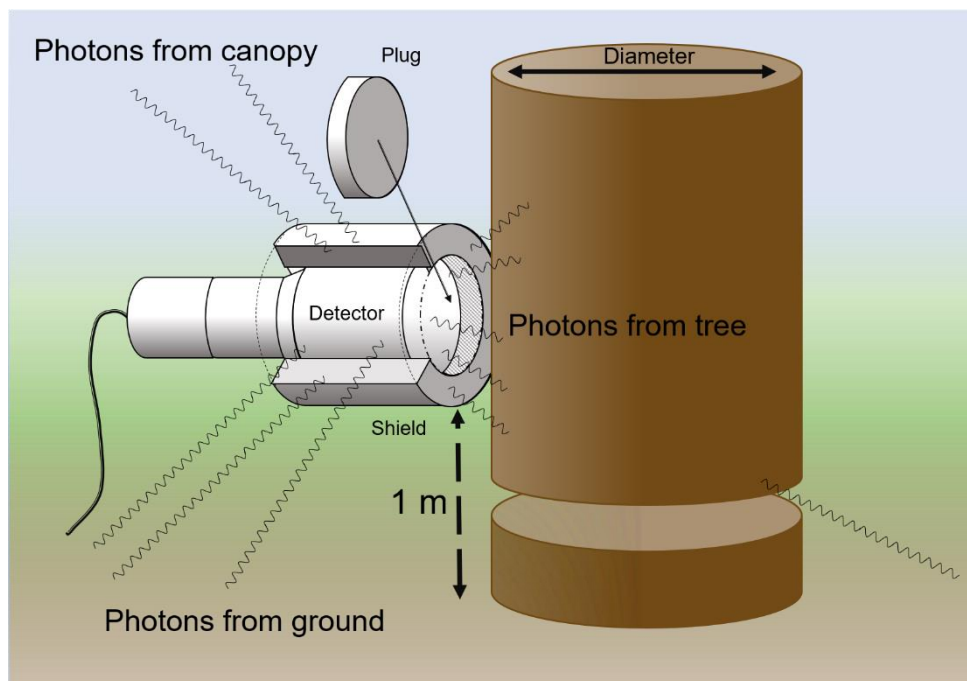
92 The next step is to take two or more separate measurements and try to separate the individual  
93 components of the signal using mathematical techniques. This study explores an approach  
94 employing strategically placed lead shielding around and in front of the detector to collimate  
95 the signal from the tree, thus reducing background signal and canopy signal and ultimately  
96 increasing the signal to noise ratio. Crucially, this setup ensures the detector remains in a  
97 constant position, negating any issues associated with changes in background and wood  
98 heterogeneity. In the past, a similar technique has been adopted with in situ gamma-ray  
99 spectrometry, wherein lead shielding was used to collimate the detector's field of view to assess  
100 the  $^{137}\text{Cs}$  depth distribution (Benke and Kearfott, 2002). The depth of burial was also estimated  
101 by using a faceplate to change the angular response of the detector to the source (Feng et al.,  
102 2012).

103 The aim of this study was to develop a system that can quickly estimate the  $^{137}\text{Cs}$  concentration  
104 within the wood of the tree for a more efficient means of identifying trees that could be felled  
105 for economic exploitation and reduce the need for intrusive sampling. The approach utilises  
106 Monte Carlo simulations to model the gamma photon spectra to identify the optimal geometries  
107 and shielding requirements for differing thicknesses of the tree and distribution of  $^{137}\text{Cs}$   
108 throughout a tree trunk. Calibration factors were derived from simulations alongside the  
109 development of regular algebraic solutions to allow careful separation of ground and tree  
110 contributions. The approach to estimate  $^{137}\text{Cs}$  activity is validated from samples taken of trees  
111 measured using the shielded detector.

112 **2. Methods**

113 *2.1. Measurement procedure and spectral processing*

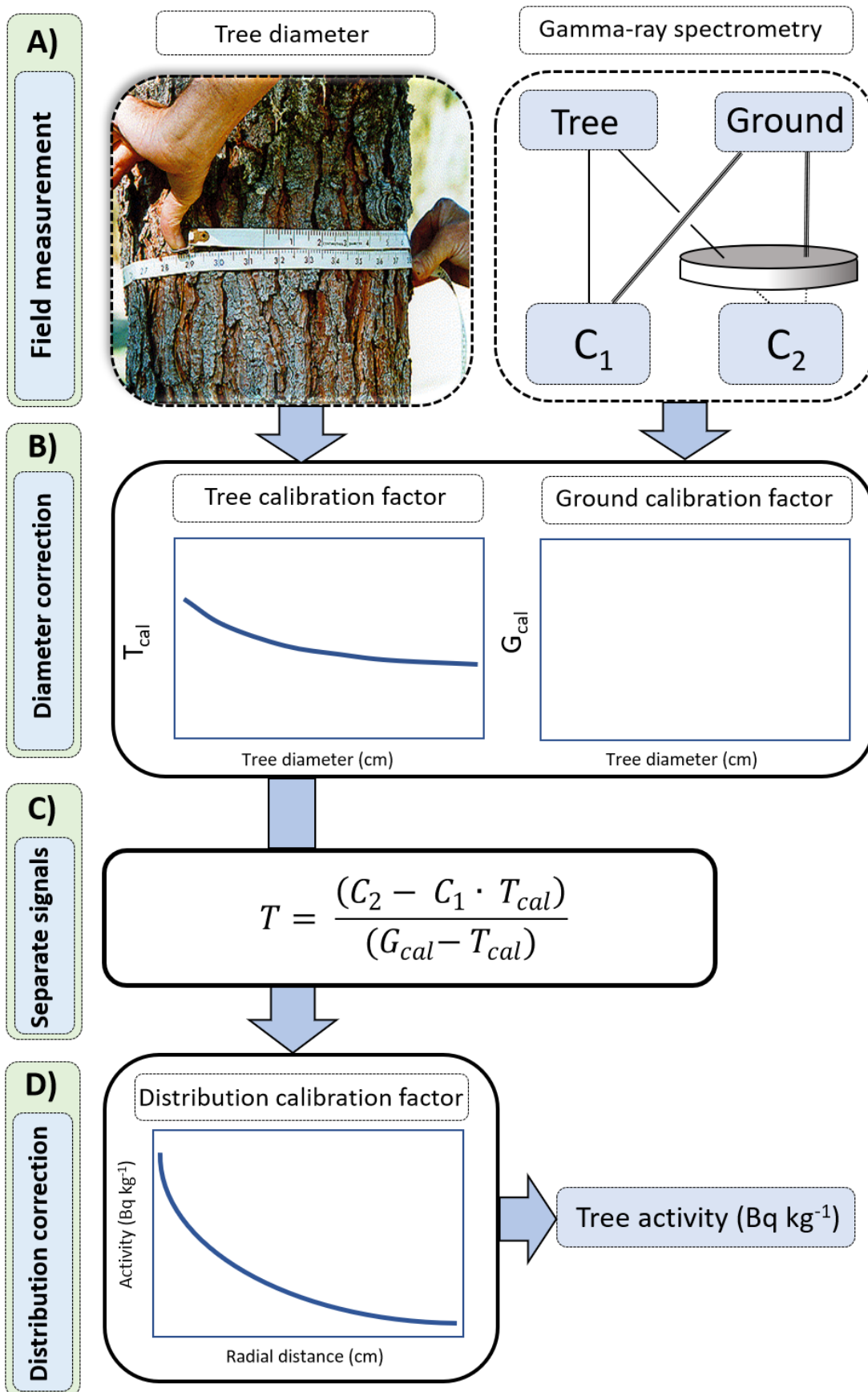
114 The first step in the measurement process involves measuring the circumference of the tree to  
115 be used in the calculation of calibration coefficients to account for its diameter (Graphical  
116 abstract - A). The sodium iodide detector is then fastened to the tree trunk at a height of a 1 m  
117 and the first measurement is taken with the lead shield open (without the front face plug),  
118 exposing the tree to the detector, the face of which is positioned 2 cm back from the front of  
119 the lead collimator (Figure 1).



120

121 Figure 1. Schematic drawing of the detector, lead collimator and plug.

122 This measurement produces the count rate  $C_1$ ; referred to as the unshielded measurement,  
123 which is made up of counts derived from the ground ( $G$ ) and Tree ( $T$ ) (Eq. 1). The second  
124 measurement is made when the plug is placed in the collimator and aims to eliminate as much  
125 of the tree signal as possible and the resultant signal can be considered as a background (Figure  
126 2A). Nevertheless, significant contributions from both ground and tree will still be observed in  
127 the count rate ( $C_2$ ) that need to be characterised using separate ground and tree calibration  
128 coefficients,  $G_{cal}$  and  $T_{cal}$ , respectively (Eq. 2).



129

130 Figure 2. Flow diagram describing the in situ measurement of  $^{137}Cs$



131

$$C_1 = G + T \quad (1)$$

132

$$C_2 = G \cdot G_{cal} + T \cdot T_{cal} \quad (2)$$

133 Derivation of calibration coefficients is performed in the second step and account for the  
134 shielding effect of the tree and plug (Figure 2B). The shielding effect from the plug is relatively  
135 constant yet changes in tree diameter will have two effects on the number of photons in both  
136  $C_1$  and  $C_2$  (eq. 1 and 2). Photons coming from the tree will generally increase with increasing  
137 tree diameter, given that there is more source volume contributing photons although the source  
138 distance will be larger for photons from the edges of the tree. At the same time, counts coming  
139 from the ground will generally decrease with increasing thickness as the tree will be providing  
140 more shielding for photons coming from behind the tree. Acting in combination, these two  
141 effects are likely to have a nonlinear relationship with tree diameter. Consequently, the  
142 relationship between the ratio of shielded and unshielded counts must be characterised in  
143 sufficient detail across a range of diameters forming two calibration coefficients  $G_{cal}$  and  $T_{cal}$   
144 where  $G_{cal}$  is the ratio between unshielded ( $G_U$ ) and shielded ( $G_S$ ) ground counts, and  $T_{cal}$  is the  
145 ratio between unshielded ( $T_U$ ) and shielded ( $T_S$ ) tree counts described in equation's 3 and 4,  
146 respectively. Essentially, each calibration coefficient is a fraction of the unshielded count.

147

$$G_{cal} = \frac{G_U}{G_S} \quad (3)$$

148

$$T_{cal} = \frac{T_U}{T_S} \quad (4)$$

149 In the third stage, equations (1) and (2) can be combined and rearranged allowing for separation  
150 of the tree signal ( $T$ ) (eq. 5) (Figure 2C).  $T$  represents the number of counts received by the  
151 detector, originating from the tree in the unshielded measurement and can be converted into  
152 activity using Monte Carlo simulations.

153

$$T = \frac{(C_2 - C_1 \cdot T_{cal})}{(G_{cal} - T_{cal})} \quad (5)$$

154 Prior to this crucial step, a correction factor must be applied to  $T$  to account for the radial  
 155 distribution in the tree (Figure 2D). The observed radial distribution within a tree is due to a  
 156 number of factors including deposition rates and soil type (Soukhova et al., 2003), although  
 157 the primary driving force is believed to be due to the biological mobility of radiocaesium within  
 158 wood, which is dependent on the species and age of the tree. In general, accumulation of  
 159 caesium tends to occur in the bark and newer growth close to the phloem through which  
 160 nutrients are transported to the roots. Contrastingly, lower concentrations are found in the pith  
 161 and older wood towards the centre where water is transferred up to the crown and into the  
 162 leaves. Importantly, differences in radial distribution can significantly influence the count rate  
 163 received by the detector and considerable caution must be applied during the application of any  
 164 correction factors.

$$A = P + (A_0 - P)e^{-cd} \quad (6)$$

165 From information gained from field observations, and literature values, a simplified model  
 166 described by an exponential function was used to model caesium radial distribution to correct  
 167 count rate to activity (Eq. 6). Activity ( $A$ ) was predicted at radial depth ( $d$ ) reducing according  
 168 to the decay constant ( $c$ ), where  $A_0$  is the activity of the outer layer of bark and  $P$  is the activity  
 169 in the pith. A visual example of a radial distribution is provided in Figure 2 in the  
 170 supplementary materials using values of 1.5 and 0.1 for  $c$  and  $P$ , respectively. Although this  
 171 distribution would suggest that contributions from the bark would have a significant effect on  
 172 the count rate, it has been calculated that less than 4 % of the counts originate from the bark  
 173 for this distribution. For larger diameters it is significantly less than 4 %. Importantly, even  
 174 though the bark is closer to the detector, its relatively small mass contributes relatively little to  
 175 the overall count rate compared to the rest of the tree.

## 176 2.2. Monte Carlo simulations

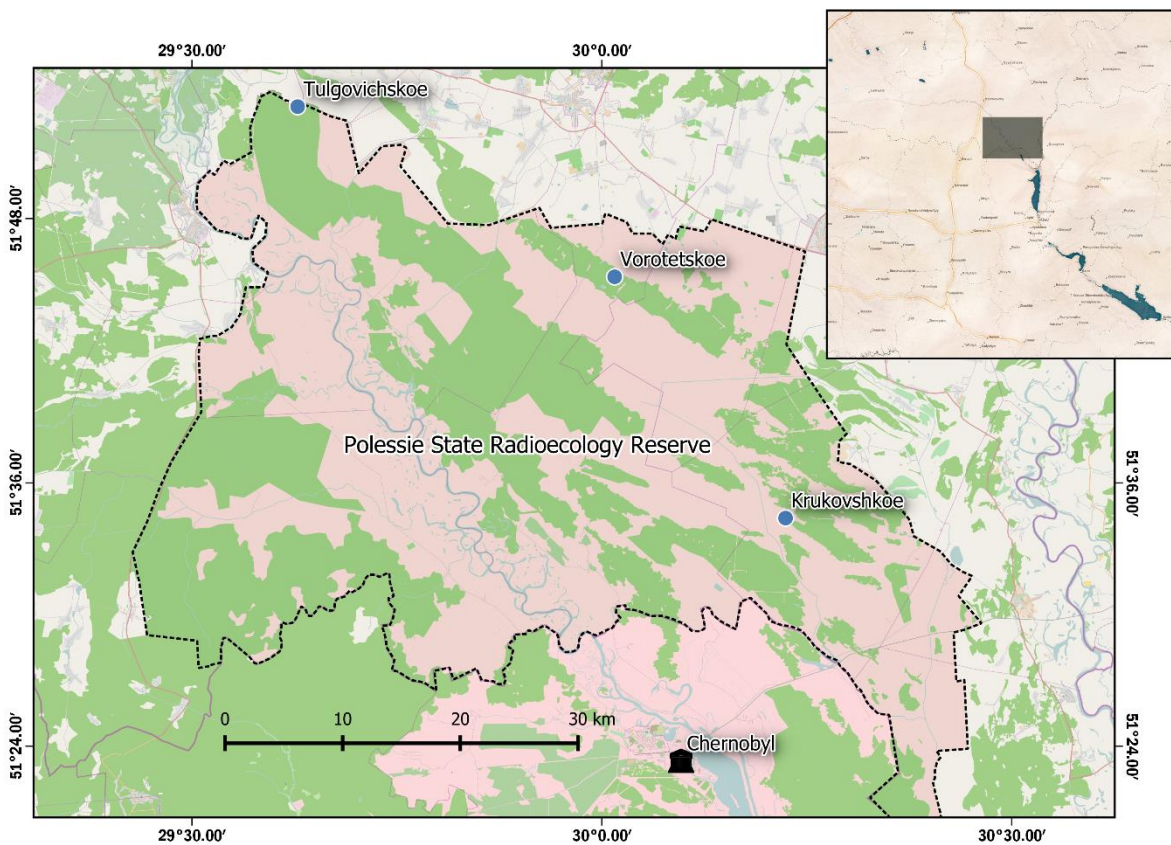
177 Calibration of the detector was performed using Monte Carlo simulations, which allowed for  
 178 complex parameters such as tree diameter and radial distribution to be changed that would  
 179 otherwise be unfeasible to do so through traditional analytical calibration procedures. A

180 detailed description of the modelling stage, including geometry specifications and processing  
181 routines can be found in the supplementary materials.

182 *2.3. Field sites and measurement*

183 To test the approach, three field sites were selected within the PSRER in the Gomel region of  
184 Belarus. The areas were specifically chosen as they covered a broad range of caesium  
185 depositions. The chosen three locations were Tulgovichskoe (low activity), Vorotetskoe  
186 (medium activity) and Krukovskoe (high activity). Locations of the three sites relative to the  
187 Chernobyl NPP are shown in Figure 3 with further details provided in Table 2 supplementary  
188 materials; based on five soil samples and corresponding dose rate measurements at each site.

189



190

191 Figure 3. Three test sites relative to the Chernobyl NPP. The dashed line indicates the boundary  
192 of the Polessie Radiation Ecology Reserve.

193

194 The Tulgovichskoe site was being actively logged as the stands at the site were deemed to be  
195 under the relevant regulatory limits (Table 1), whereas the Vorotetskoe and Krukovskoe sites  
196 had been untouched since 1986 as they were considered near to or over Belarussian statutory  
197 limits with respect to  $^{137}\text{Cs}$  content ( $740 \text{ Bq kg}^{-1}$ ). A rectangular area (approximately  $30 \times 30$   
198 m) in which the dose rate was deemed to be the most stable spatially was identified at each of  
199 the three forestry sites. The spatial distribution of  $^{137}\text{Cs}$  was mapped at each site using a  $76 \times$   
200  $76 \text{ mm NaI:Tl}$  detector integrated with a high accuracy DGPS which provided reliable accuracy  
201 under trees for 30 minutes once a signal had been attained. Individual spectra were converted  
202 to  $^{137}\text{Cs}$  inventory by following the procedure outlined in Varley et al. (2017).

203 Within the selected mapped areas, 10 mature trees were randomly chosen to test the in situ  
204 method and a subset of 4 trees was randomly selected for wood and bark sampling prior to the  
205 in situ gamma-ray measurement. Trees were randomly selected by randomly generating  
206 coordinates in the map and selecting the closest tree to that coordinate. Wood samples were  
207 taken with a tree corer (Haglöf, 5.15 mm diameter, length 300 mm). The remaining 6 trees  
208 were not physically sampled, but in situ measurements were performed. Three trees from the  
209 Vorotetskoe and Krukovskoe sites were felled to serve as test logs: one pine (*Pinus sylvestris*)  
210 from Vorotetskoe, one pine from Krukovskoe and one birch (*Betula pendula*) from  
211 Vorotetskoe. The felled trees were moved to an unforested area of low  $^{137}\text{Cs}$  activity ( $\sim 333 \text{ Bq}$   
212  $\text{kg}^{-1}$ ) producing negligible counts from the background. This area was referred to as the test  
213 facility. Samples were taken from tests logs from the duramen (dead, central heartwood) and  
214 the alburnum (the living secondary sapwood) using a chainsaw alongside bark samples taken  
215 with an axe. Samples of each of these three materials were then analysed by HPGe in the  
216 laboratory for  $^{137}\text{Cs}$  content.

217 In situ measurements were taken with an Inspector<sup>TM</sup> 1000 from Canberra and count times  
218 were of the order of 3 – 5 minutes, typically resulting in a counting uncertainty under the full  
219 energy peak at 661 keV of below 2%.

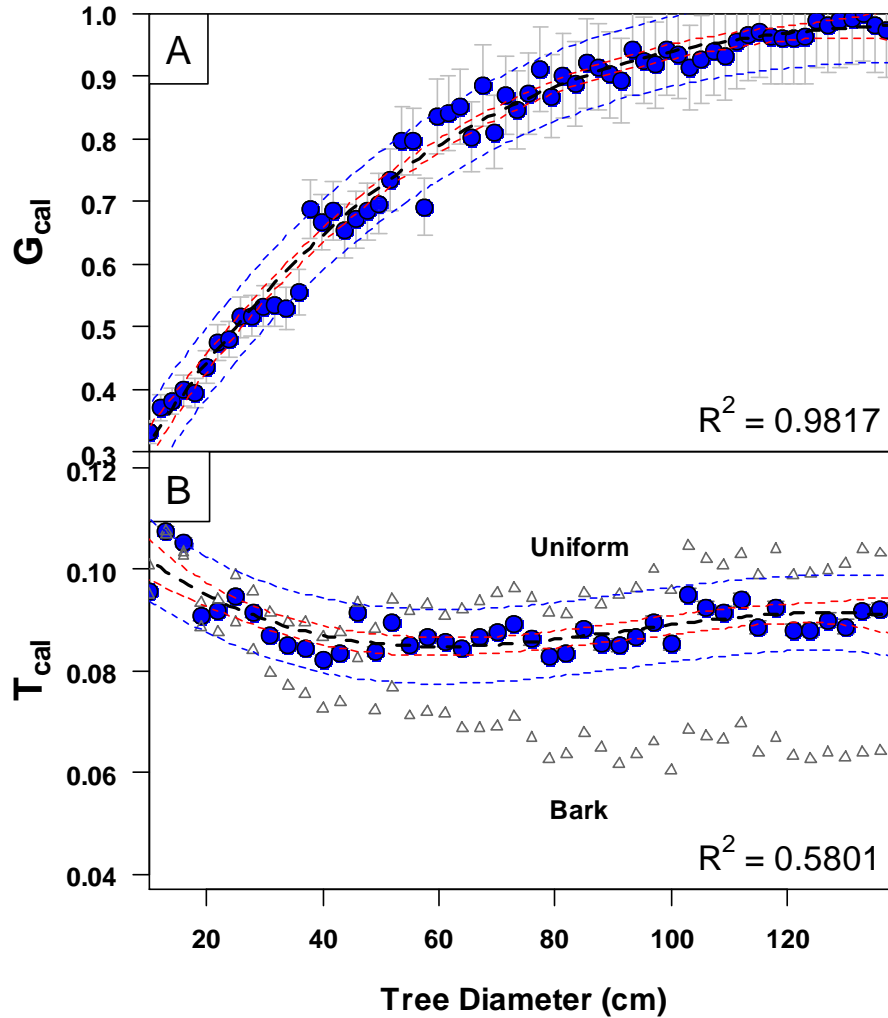
## 220 3. Results and Discussion

### 221 3.1. Monte Carlo results

222 Tree and ground results derived from Monte Carlo give insight into how the detection system  
223 interacts with the shield, plug, ground and tree (Figure 4). For the ground model changes in  
224 tree diameter effectively introduce shielding and this can be realised as a gradual decrease in  
225 the number of counts entering through the front face of the detector in the unshielded ( $G_U$ )  
226 measurement. Concurrently, this has less of an effect on the shielded measurement ( $G_S$ ) as it is  
227 already partially shielded by the plug. Acting in combination to produce the value  $G_{cal}$ , the ratio  
228 between  $G_U$  and  $G_S$  effectively enters a state of equilibrium ( $G_{cal} = 1$ ) at around 120 cm, as this  
229 thickness of the tree effectively shields all photon coming from the front face (Figure 4A).  
230 Across a typical tree diameter range,  $G_{cal}$  can vary by up to 70 %. Importantly, it is this  
231 relationship that allows the method to work and for the signal to be separated. The diameter of  
232 the tree can be inputted into the model and for a certain diameter of tree, the drop in count rate  
233 can be predicted from  $G_{cal}$  leaving the tree count rate.

234 It is a different case for  $T_{cal}$ , where the influence of the tree diameter has very little effect on the  
235 ratio between unshielded ( $T_U$ ) and shielded ( $T_S$ ) measurements, where only minor variations in  
236  $T_{cal}$  are witnessed (8 - 10 %) across the diameter range (Figure 4B). Notice that the radial  
237 distribution can have a slight influence on  $T_{cal}$ , for example the difference between a uniform  
238 and a distribution mostly associated with the bark. Yet, in terms of potential uncertainty, this is  
239 low in comparison to the final calibration stage in Eq 6, where large variations in radial depth  
240 distribution could introduce orders of magnitude of change in the count rate for the same overall  
241 activity.

242



243

244 Figure 4. Model fits derived from Monte Carlo data for ground (A) and tree (B) calibration  
 245 factors,  $G_{cal}$  and  $T_{cal}$ , as a function of tree diameter. Fitted polynomial models display both  
 246 confidence (red broken lines) and prediction (blue lines) intervals at 95% and error bars  
 247 represent counting uncertainty ( $1\sigma$ ). Triangles show the influence of tree diamtere on  $T_{cal}$  when  
 248  $^{137}\text{Cs}$  is either distributed uniformly throughout the trunk or located predominantly in the bark.

### 249 3.2. Test logs

250 To test the performance of the detector and shield within a relatively controlled environment,  
 251 measurements were taken from three test logs (taken from high activity areas) over relatively  
 252 low activity ground. In this scenario, the count rate from the log was many orders of magnitude  
 253 higher than the background. These controlled conditions allowed Monte Carlo results derived  
 254 purely for the tree to be assessed without significant contribution from the ground and  
 255 importantly provide verification for the distribution model.

256 Observing the ratio between duramen (heartwood) and alburnum (sapwood) <sup>137</sup>Cs  
 257 concentrations in wood tissue between the pine logs and birch logs confirmed that the trees  
 258 have different radial distributions, but still contain higher contamination towards the outside of  
 259 the tree in the living wood and the bark (Table 4 in supplementary material). By analysing the  
 260 duramen/alburnum ratio it becomes clear that contamination within pine species (0.442-0.482)  
 261 tends to be closer to the bark of the tree compared to the birch tree (1.080-1.230) (Table 2).  
 262 This finding matches general patterns found by other studies on distributions of this isotope in  
 263 trees (Ohashi et al., 2014; Soukhova et al., 2003). The limited sample size was not enough to  
 264 draw significant conclusion on radial distribution but was enough to approximately  
 265 parameterise Monte Carlo models to derive activity estimates from in situ count rates.

266 Table 2. Cs-137 activity concentrations in various radial sections of the test logs based on  
 267 laboratory measurement. Measurement uncertainties 2σ for laboratory and *in situ*  
 268 measurements.

Test log	Average wood activity (Bq kg <sup>-1</sup> )	In situ estimate (Bq kg <sup>-1</sup> )	Duramen/alburnum activity concentration ratio
Pine (Krukovskoe) – base of log	4220 ± 1200	4260 ± 1350	0.442
Pine (Krukovskoe) – top of log	5170 ± 1460	5200 ± 1800	0.456
Pine (Vorotetskoe) – base of log	841 ± 249	816 ± 315	0.482
Pine (Vorotetskoe) – top of log	619 ± 182	664 ± 249	0.454
Birch (Vorotetskoe) – base of log	551 ± 157	716 ± 283	1.080
Birch(Vorotetskoe) – top of log	452 ± 131	507 ± 205	1.230

269 Laboratory results from wood samples taken from the test facility were compared to  
 270 measurements made along the logs using the in situ detector (Table 2). In situ measurements  
 271 were calibrated using the conservative parameters from the radial distribution data for the pine  
 272 test logs. It was decided that due to the potentially more complex distribution within the birch  
 273 trees, and the smaller amount of data available, the pine distribution would be fitted to the birch  
 274 tree results. Furthermore, the pine distribution was more relevant to this study as most of the  
 275 trees that were measured in the field were Scots Pine trees.

276 Wood samples and in situ activity estimates were within 7 % of each other for the test pine logs.  
 277 Wood activity estimates for the birch log were less reliable (< 25 %), this is understandable  
 278 given that the exponential radial distribution that was fitted to the pine data will be different  
 279 compared to that of a typical birch radial distribution (Table 2).

280 3.3. *Soil transfer factors*

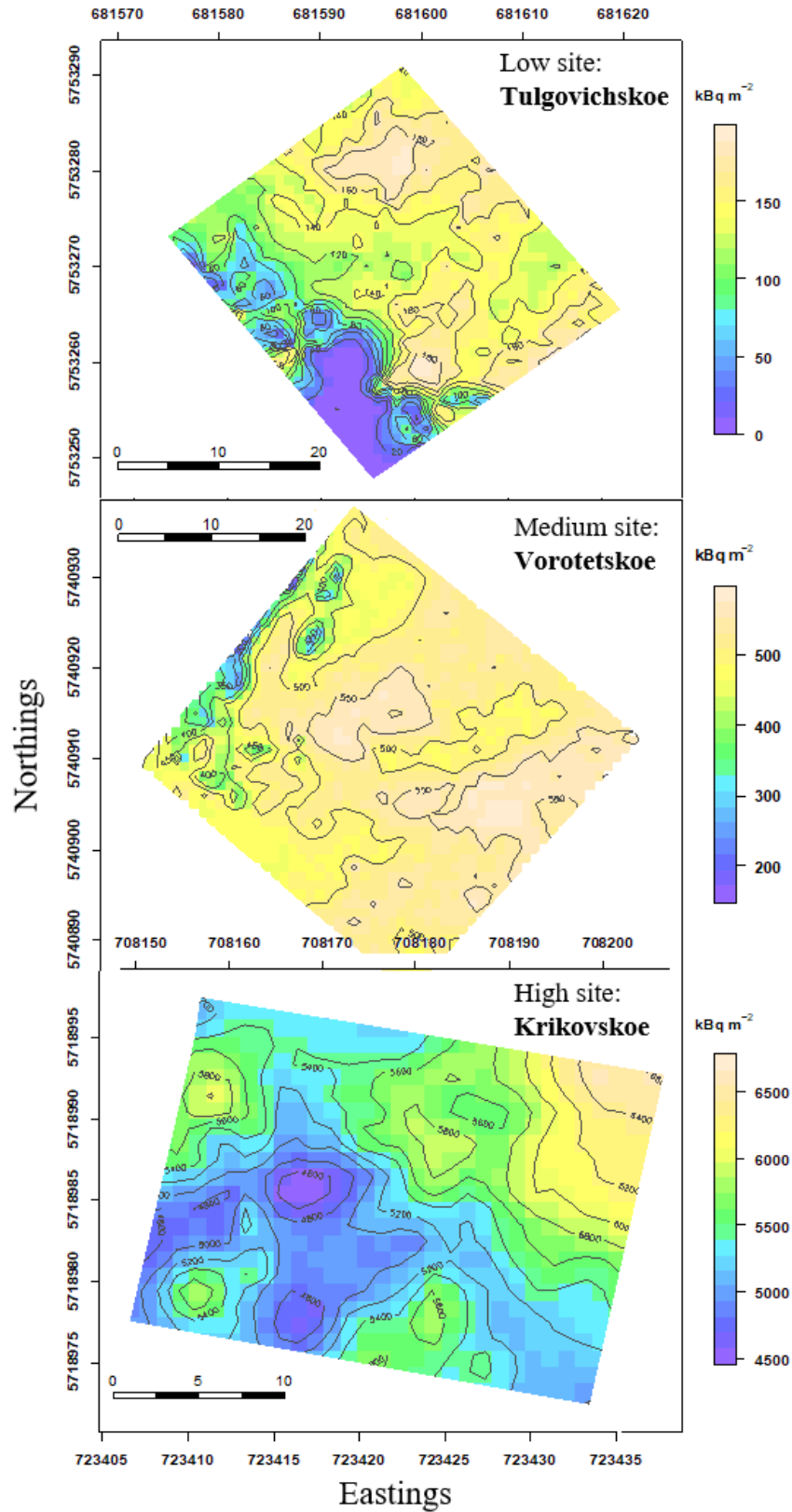
281 As discussed earlier, the conventional way of estimating activity levels in trees is by use of  
282 concentration ratios. A statistical summary of  $^{137}\text{Cs}$  concentration ratios for various groups of  
283 relevance to this study is shown in Table S2 in the supplementary materials which was extracted  
284 from IAEA (2014).

285 The most suitable values to apply were from the category ‘Trees: broad-leaf’ for birch and  
286 ‘Trees coniferous’ for pine, albeit that essentially identical concentration ratios are provided for  
287 both categories. The underlying datasets used to derive transfer factors are generally considered  
288 to be characterised by log-normal distributions (Sheppard, 2005) and thus the geometric mean  
289 provides the most appropriate selection for a best estimate or central tendency of the CR value  
290 (see Table S3 in the supplementary materials).

291 3.4. *Field site deposition patterns*

292 Although site selection aimed to find 3 areas that were relatively spatially uniform, mapped by  
293 mobile gamma-ray spectroscopy results, indicate that there was considerable heterogeneity  
294 across all 3 sites Figure 5 . This is not a surprising result given that across much of the exclusion  
295 zone contamination tends to be heterogeneous and can be difficult to characterise without  
296 equipment such as a mobile gamma-ray spectrometry operating a spatially sensitive differential  
297 GPS. Although not displayed, little difference in  $^{137}\text{Cs}$  depth distribution, derived using the  
298 peak-to-valley ratio, was found within each site. Between sites there was also not a significant  
299 difference in depth. Most of the contamination was estimated to be within the top 10 cm of the  
300 soil surface





301

302 Figure 5. Spatial distribution of <sup>137</sup>Cs at each of the three sites chosen for the study.

303 The capability to map contamination at high spatial resolution raises potential issues in using  
304 transfer factor approaches that rely on a small amount of soil samples to statistically derive soil  
305 activity. At each of the three sites, clearly issues could be encountered using a limited soil  
306 sampling size within a heterogeneous environment. In this scenario, the true value of mobile  
307 gamma-ray spectrometry becomes clear, as these measurements by themselves could quite  
308 easily be used to inform transfer factors and provide a rapid means of characterising forest  
309 stands. After which measurements could be used to target the in situ method on specific trees.

### 310 3.5. *Wood activity estimates*

311 In general, good agreement is seen between in situ wood activity estimates ( $\text{Bq kg}^{-1}$ ) and wood  
312 activities taken using coring device (Table 3). In particular ID 1-5, taken at the high activity  
313 site (Krukovskoe) shows a deviation of less than 20 % with exception of ID 3 (~50 % deviation).  
314 This high level of agreement could be attributed to the diameter of the trees being relatively  
315 small and being relatively consistent across the site. Not only did this make in situ  
316 measurements easier and the modelling process more straightforward, but the corer could reach  
317 closer to the centre of the tree providing a representative sample of wood throughout the radial  
318 distribution and would result in more consistency between trees. Furthermore, a low counting  
319 uncertainty could be achieved in a relatively short amount of time due to the high levels of  
320 contamination.

321 Trees that were measured using the *in situ* detector, but did not have corresponding wood  
322 sample data, still adhered closely to wood activity estimates from nearby trees for which wood  
323 sample data was available suggesting that wood activity was reasonably consistent across the  
324 site (3200-5330  $\text{Bq kg}^{-1}$ ). The variability present at this site is, interestingly, comparable to the  
325 variability shown across the site from that identified using mobile gamma-ray spectrometry  
326 (Table 5 in the supplementary materials). GPS coordinates taken in the field to mark trees were  
327 accrued using a standard GPS without differential correction and were not reliable enough to  
328 allow for direct comparison.

329 Activities estimated from the medium activity site (Vorotetskoe) were for the most part  
330 reflective of wood sampling estimates (~20 %) for IDs 12-14. In situ estimates for ID 15 were  
331 considerably different to the wood estimate (>55 %). This disparity could be caused by the trees  
332 especially large diameter meaning that the 300 mm coring device probably significantly under  
333 sampled the middle of the tree taking relatively more of the higher activity wood present in the

334 sapwood. Examination of the rest of the in situ measurements without matching wood sample  
335 data tends to support this argument as many of the predicted wood activities were between 382-  
336 529 Bq kg<sup>-1</sup> (Table 3).

337 The least comparable results were found at the lowest activity site. Notice that the in situ  
338 estimate ( $125 \pm 44$  Bq kg<sup>-1</sup>) for ID 21 is over 2 times that of the wood estimate ( $54 \pm 12$  Bq kg<sup>-1</sup>).  
339 However, these results were proved not to be significantly different using a one-way  
340 ANOVA. Interestingly this was the only birch tree measured in the field and, in concurrence  
341 with the test logs, an overestimate of activity was found. This is most likely a consequence of  
342 the model being inappropriate for the birch tree radial distribution as it was fitted to pine tree  
343 data. However, further deviations of 100 % were found for the remaining two pine trees,  
344 although these were not found to be significantly different. These results are harder to explain  
345 as the wood sample estimates are lower than the in situ estimates, which cannot be explained  
346 by the larger diameters of the trees such as the case at the medium site. Ascertaining the exact  
347 reason for this outcome is difficult, although perhaps the low count rates at this site played a  
348 significant role and increased uncertainty. Another possibility is that the radial distribution  
349 could have been considerably different at this site as is the forest stand was visually very  
350 different and contained a greater diversity of trees and had a different soil type. It is evident that  
351 further research is required to resolve this issue.

352 Estimates made using the TR method were fairly robust in terms of encapsulating the maximum  
353 and minimum bounds of the wood sampled activity estimates and the in situ and mobile gamma-  
354 ray spectrometry activity estimates. It is understandable why TR are widely adopted  
355 particularly if there are only soil activity estimates available.

356

357

358

359

360

361

362

363

364 Table 3. Wood activity at field sites derived from wood cores, in situ measurements and  
 365 transfer factors. Measurement uncertainties are quoted to  $2\sigma$ .

Site	ID	Tree circumference (cm)	Species	Core samples	In situ	Transfer factor
				Wood activity (Bq kg <sup>-1</sup> )	Wood activity (Bq kg <sup>-1</sup> )	Wood activity (Bq kg <sup>-1</sup> )
Krukovskoe	1	141	Pine	<b>3410 ± 705</b>	<b>3310 ± 1050</b>	<b>2040 – 6350</b>
Krukovskoe	2	122	Pine	<b>3200 ± 680</b>	<b>3930 ± 1270</b>	<b>2040 – 6350</b>
Krukovskoe	3	122	Pine	<b>3200 ± 680</b>	<b>4900 ± 1610</b>	<b>2040 – 6350</b>
Krukovskoe	4	96	Pine	<b>4010 ± 840</b>	<b>4490 ± 1550</b>	<b>2040 – 6350</b>
Krukovskoe	5	82	Pine	<b>3600 ± 750</b>	<b>4280 ± 1452</b>	<b>2040 – 6350</b>
Krukovskoe	6	117	Pine	-	4160 ± 1400	2040 – 6350
Krukovskoe	7	118	Pine	-	3270 ± 1200	2040 – 6350
Krukovskoe	8	138	Pine	-	3200 ± 1010	2040 – 6350
Krukovskoe	9	119	Pine	-	4110 ± 1370	2040 – 6350
Krukovskoe	10	87	Pine	-	5330 ± 2010	2040 – 6350
Krukovskoe	11	120	Pine	-	3670 ± 1220	2040 – 6350
Vorotetskoe	12	114	Pine	<b>578 ± 123</b>	<b>521 ± 177</b>	<b>260 - 545</b>
Vorotetskoe	13	169	Pine	<b>575 ± 125</b>	<b>463 ± 162</b>	<b>260 - 545</b>
Vorotetskoe	14	169	Pine	<b>575 ± 125</b>	<b>445 ± 156</b>	<b>260 - 545</b>
Vorotetskoe	15	178	Pine	<b>1010 ± 209</b>	<b>435 ± 158</b>	<b>260 - 545</b>
Vorotetskoe	16	114	Pine	-	593 ± 201	260 - 545
Vorotetskoe	17	111	Pine	-	417 ± 143	260 - 545
Vorotetskoe	18	112	Pine	-	382 ± 131	260 - 545
Vorotetskoe	19	89	Pine	-	518 ± 194	260 - 545
Vorotetskoe	20	99	Pine	-	529 ± 190	260 - 545
Tulgovichskoe	21	110	Birch	<b>54 ± 12</b>	<b>125 ± 44</b>	<b>60 - 112</b>
Tulgovichskoe	22	152	Pine	<b>48 ± 11</b>	<b>96 ± 29</b>	<b>60 - 112</b>
Tulgovichskoe	23	152	Pine	<b>48 ± 11</b>	<b>94 ± 29</b>	<b>60 - 112</b>
Tulgovichskoe	24	213	Pine	<b>67 ± 16</b>	<b>70 ± 19</b>	<b>60 - 112</b>
Tulgovichskoe	25	211	Oak	-	87 ± 23	60 - 112
Tulgovichskoe	26	185	Pine	-	65 ± 18	60 - 112
Tulgovichskoe	27	169	Pine	-	76 ± 23	60 - 112

Matched data are displayed in bold

### 366 3.6. Future directions

367 It is clear from the findings of this study that being able to rapidly measure activity activity  
 368 concentrations of <sup>137</sup>Cs across the site and in wood using non-destructive *in situ* gamma-ray  
 369 spectrometry represents a considerable step forward in characterising contaminated forests such

370 as those found in the Polessie State Radioecology Reserve. The methods capability could  
371 certainly become a useful prospecting tool for the forestry industry that could improve decision  
372 making as to whether a tree should be felled or not depending on specified regulatory limits.  
373 Such an approach might conceivably comprise two phases: (i) in situ or mobile mapping the  
374 understory soil contamination levels to highlight likely areas for felling followed by  
375 (ii) measurements of tree activity for verification through in situ measurements coupled with a  
376 subset of trees being subject to laboratory measurement validation.

377 The outstanding uncertainties identified by this study were found to be the radial distribution  
378 of the contaminant within trees of different species and wood density, which were modelled  
379 from preliminary field and literature observations. Understanding how these environmental  
380 parameters drive the observed count rate of the system is the next crucial step. For example,  
381 accurate characterisation of green wood density is necessary for each individual measurement,  
382 although this could be feasibly determined in field using tree cores or modelled using historical  
383 data.

384 Perhaps a more demanding challenge is to reliably account for changes in radial distribution.  
385 To accomplish this, large amounts of empirical data will have to be acquired to investigate  
386 patterns in the shape of the radial distribution for a given species considering the age and  
387 diameter of the tree and perhaps the underlying soil distribution. Current estimates from the  
388 models developed in this study suggest that without confident resolution of this parameter final  
389 wood activity estimates could be orders of magnitude from the true value and no better than  
390 estimates of transfer factors, albeit without the need for physical sampling. Although  
391 discrepancies between *in situ* and coring estimates were not found to be to this level within this  
392 study, differences at the low activity site could in part be explained by this occurrence.

393 A final argument for the further development of this *in situ* method is the unpredictability of  
394 the core data taken during this study. The results suggest that *in situ* results could in fact be  
395 more representative of the true activity value, by showing less statistical variation, than the core  
396 values that were used to validate due to the consistency in results displayed across each site.

397 It must be noted,  $^{137}\text{Cs}$  poses less risk to human health compared with  $^{90}\text{Sr}$  with regards to wood  
398 contamination as strontium is absorbed more readily by trees. However,  $^{90}\text{Sr}$  is more difficult  
399 to measure in situ as it does not have a significant gamma-ray emission, therefore is only  
400 feasible to measure through laboratory equipment.

401 **4. Conclusions**

402 A non-destructive in situ gamma spectrometric method to measure  $^{137}\text{Cs}$  contamination in trees  
403 has been described and demonstrated in a forest in the Belarusian Chernobyl exclusion zone.  
404 The real-time method showed promising agreement with wood activity estimates made using a  
405 traditional tree coring device and laboratory gamma-ray spectrometry. Potentially, the method  
406 could be widely adopted, alongside mobile gamma-ray spectrometry, negating the need for a  
407 tree to be felled and prolonged laboratory measurement of sampled environmental media.  
408 Wider investigations into the uncertainties distributions associated with wood density and radial  
409 distribution are required. Larger scale datasets are required to parameterise the underlying  
410 models used to separate the signal from the tree and the background and the final radial  
411 distribution calibration factor to derive wood activity.

412 **Acknowledgements**

413 The authors are grateful to the workers of the scientific part of the Polesie State Radiation  
414 Ecology Reserve: V. Kalinin, E. Kalyhan, N. Dzemenkavets, A. Masheuski, N. Blinova, A.  
415 Uhljanets and D. Garbaruk for fieldwork, sample preparation and laboratory analysis.

416

417

418

419

420

421

422 **5. References**

- 423 Auty, D., Achim, A., Macdonald, E., Cameron, A.D., Gardiner, B.A., 2014. Models for  
424 predicting wood density variation in Scots pine. *Forestry* 87, 449–458.  
425 <https://doi.org/10.1093/forestry/cpu005>
- 426 Beck, H., DeCampo, J., Gogolak, C., 1972. In situ Ge(Li) and NaI(Tl) gamma-ray spectrometry.  
427 New York. <https://doi.org/10.2172/4599415>
- 428 Benke, R.R., Kearfott, K.J., 2002. Demonstration of a collimated in situ method for determining  
429 depth distributions using g-ray spectrometry, *Nuclear Instruments and Methods in Physics*  
430 *Research A*.
- 431 Briesmeister, J.F., 1993. MCNP-A general Monte Carlo N-particle transport code. LA-12625.
- 432 Cresswell, A.J., Kato, H., Onda, Y., Nanba, K., 2016. Evaluation of forest decontamination  
433 using radiometric measurements. *J. Environ. Radioact.* 164, 133–144.  
434 <https://doi.org/10.1016/j.jenvrad.2016.07.024>
- 435 de Groot, A. V., van der Graaf, E.R., de Meijer, R.J., Maučec, M., 2009. Sensitivity of in-situ  
436  $\gamma$ -ray spectra to soil density and water content. *Nucl. Instruments Methods Phys. Res. Sect.*  
437 *A Accel. Spectrometers, Detect. Assoc. Equip.* 600, 519–523.  
438 <https://doi.org/10.1016/j.nima.2008.12.003>
- 439 Dvornik, A.A., Dvornik, A.M., Korol, R.A., Shamal, N. V., Gaponenko, S.O., Bardyukova, A.  
440 V., 2018. Potential threat to human health during forest fires in the Belarusian exclusion  
441 zone. *Aerosol Sci. Technol.* 52, 923–932.  
442 <https://doi.org/10.1080/02786826.2018.1482408>
- 443 Evangeliou, N., 2015. Fire evolution in the radioactive forests of Ukraine and Belarus: future  
444 risks for the population and the environment. *Ecol. Monogr.* 85, 49–72.
- 445 Feng, T.C., Jia, M.Y., Feng, Y.J., 2012. Method-sensitivity of in-situ gamma spectrometry to  
446 determine the depth-distribution of anthropogenic radionuclides in soil. *Nucl. Instruments*  
447 *Methods Phys. Res. Sect. A-Accelerators Spectrometers Detect. Assoc. Equip.* 661, 26–  
448 30. <https://doi.org/10.1016/j.nima.2011.09.014>

- 449 Fogh, C.L., Andersson, K.G., 2001. Dynamic behaviour of <sup>137</sup>Cs contamination in trees of the  
450 Briansk region, Russia. *Sci. Total Environ.* 269, 105–115. <https://doi.org/10.1016/S0048->  
451 9697(00)00819-6
- 452 Gerasimov, Y., Karjalainen, Y., 2010. (PDF) Atlas of the forest sector in Belarus. Work. Pap.  
453 Finnish For. Res. Inst. 170Publisher Finnish For.
- 454 Gering, C.F., Kiefer, P., Fesenko, S., Voigt, G., 2002. In situ gamma-ray spectrometry in  
455 forests: determination of kerma rate in air from. *J. Environ. Radioact.* 61, 75–89.
- 456 Golosov, V., 2003. Application of Chernobyl-derived <sup>137</sup>Cs for the assessment of soil  
457 redistribution within a cultivated field. *Soil Tillage Res.* <https://doi.org/10.1016/S0167->  
458 1987(02)00130-7
- 459 Golosov, V.N.V., Walling, D., Kvasnikova, E.V.E., Stukin, E.D., Nikolaev, A.N., Panin, A. V.,  
460 2000. Application of a field-portable scintillation detector for studying the distribution of  
461 <sup>137</sup>Cs inventories in a small basin in Central Russia. *J. Environ. Radioact.* 48, 79–94.  
462 [https://doi.org/10.1016/S0265-931X\(99\)00058-2](https://doi.org/10.1016/S0265-931X(99)00058-2)
- 463 Goor, F., Avila, R., 2003. Quantitative comparison of models of <sup>137</sup>Cs cycling in forest  
464 ecosystems. *Environ. Model. Softw.* 18, 273–279. <https://doi.org/10.1016/S1364->  
465 8152(02)00075-0
- 466 Goor, F., Davydchuk, V., Vandenhove, H., 2003. GIS-based methodology for Chernobyl  
467 contaminated land management through biomass conversion into energy - A case study  
468 for Polessie, Ukraine. *Biomass and Bioenergy* 25, 409–421.  
469 [https://doi.org/10.1016/S0961-9534\(03\)00034-5](https://doi.org/10.1016/S0961-9534(03)00034-5)
- 470 Goor, F., Thiry, Y., 2004. Processes, dynamics and modelling of radiocaesium cycling in a  
471 chronosequence of Chernobyl-contaminated Scots pine (*Pinus sylvestris* L.) plantations.  
472 *Sci. Total Environ.* 325, 163–180. <https://doi.org/10.1016/j.scitotenv.2003.10.037>
- 473 Harrison, R.L., 2009. Introduction to Monte Carlo simulation, in: *AIP Conference Proceedings*.  
474 pp. 17–21. <https://doi.org/10.1063/1.3295638>
- 475 IAEA, 2008. Environmental consequences of the Chernobyl accident and their remediation: 20  
476 years of experience. *Chernobyl.* <https://doi.org/10.1093/rpd/ncl163>



477 Ipatyev, V., Bulavik, I., Baginsky, V., Goncharenko, G., Dvornik, A., 1999. Forest and  
478 Chernobyl: Forest ecosystems after the Chernobyl nuclear power plant accident: 1986-  
479 1994. *J. Environ. Radioact.* 42, 9–38. [https://doi.org/10.1016/S0265-931X\(98\)00042-3](https://doi.org/10.1016/S0265-931X(98)00042-3)

480 Izrael, Y.A., De Cort, M., Jones, A.R., Nazarov, I.M., Fridman, S.D., Kvasnikova, E. V., Stukin,  
481 E.D., Kelly, G.N., Matveenکو, I.I., Pokumeiko, Y.M., Tabatchnyi, L.Y., Tsaturon, Y.,  
482 1996. The atlas of caesium-137 contamination of Europe after the Chernobyl accident.  
483 *Radiol. consequences Chernobyl Accid.* 1–10.

484 Kirk, B.L., 2010. Overview of Monte Carlo radiation transport codes, in: *Radiation*  
485 *Measurements*. Pergamon, pp. 1318–1322. <https://doi.org/10.1016/j.radmeas.2010.05.037>

486 Likar, A., Vidmar, T., Lipoglavsek, M., Omahen, G., 2004. Monte Carlo calculation of entire  
487 in situ gamma-ray spectra. *J. Environ. Radioact.* 72, 163–168.

488 Malins, A., Okumura, M., Machida, M., Takemiya, H., Saito, K., 2015. Fields of View for  
489 *Environmental Radioactivity* 2–7.

490 Maučec, M., De Meijer, R.J., Van Der Klis, M.M.I.P., Hendriks, P.H.G.M., Jones, D.G., 2004.  
491 Detection of radioactive particles offshore by gamma-ray spectrometry Part II: Monte  
492 Carlo assessment of acquisition times. *Nucl. Instruments Methods Phys. Res. Sect. A*  
493 *Accel. Spectrometers, Detect. Assoc. Equip.* 525, 610–622.  
494 <https://doi.org/10.1016/j.nima.2004.01.075>

495 Maučec, M., Hendriks, P.H.G.M., Limburg, J., de Meijer, R.J., 2009. Determination of  
496 correction factors for borehole natural gamma-ray measurements by Monte Carlo  
497 simulations. *Nucl. Instruments Methods Phys. Res. Sect. A Accel. Spectrometers, Detect.*  
498 *Assoc. Equip.* 609, 194–204. <https://doi.org/http://dx.doi.org/10.1016/j.nima.2009.08.054>

499 Melin, J., Wallberg, L., Suomela, J., 1994. Distribution and retention of cesium and strontium  
500 in Swedish boreal forest ecosystems. *Sci. Total Environ.* 157, 93–105.  
501 [https://doi.org/10.1016/0048-9697\(94\)90568-1](https://doi.org/10.1016/0048-9697(94)90568-1)

502 Miller, K.M., Kuiper, J.L., Helfer, I.K., 1990. <sup>137</sup>Cs fallout depth distributions in forest versus  
503 field sites: Implications for external gamma dose rates. *J. Environ. Radioact.* 12, 23–47.  
504 [https://doi.org/10.1016/0265-931X\(90\)90034-S](https://doi.org/10.1016/0265-931X(90)90034-S)

- 505 Myttenaere, C., Schell, W.R., Thiry, Y., Sombre, L., Ronneau, C., van der Stegen de Schrieck,  
506 J., 1993. Modelling of Cs-137 cycling in forests: recent developments and research needed.  
507 Sci. Total Environ. 136, 77–91. [https://doi.org/http://dx.doi.org/10.1016/0048-](https://doi.org/http://dx.doi.org/10.1016/0048-9697(93)90298-K)  
508 9697(93)90298-K
- 509 Narayan, R.D., Miranda, R., Rez, P., 2012. Monte Carlo simulation for the electron cascade  
510 due to gamma rays in semiconductor radiation detectors. J. Appl. Phys. 111, 64910.  
511 <https://doi.org/10.1063/1.3698370>
- 512 Nimis, P.L., 1996. RADIOCESIUM IN PLANTS OF FOREST ECOSYSTEMS, Studia  
513 Geobotanica.
- 514 Ohashi, S., Okada, N., Tanaka, A., Nakai, W., Takano, S., 2014. Radial and vertical  
515 distributions of radiocesium in tree stems of *Pinus densiflora* and *Quercus serrata* 1.5 y  
516 after the Fukushima nuclear disaster. J. Environ. Radioact. 134, 54–60.  
517 <https://doi.org/10.1016/j.jenvrad.2014.03.001>
- 518 Östlund, K., Samuelsson, C., Rääf, C.L., 2015. Experimentally determined vs: Monte Carlo  
519 simulated peak-to-valley ratios for a well-characterised n-type HPGe detector. Appl.  
520 Radiat. Isot. <https://doi.org/10.1016/j.apradiso.2014.09.022>
- 521 RDU/LH-2001, 2001. Republican permissible levels of content of <sup>137</sup>Cs in wood, products  
522 from wood and wood materials and other non-edible products of forestry (in Russian).
- 523 Shaw, G., Robinson, C., Holm, E., Frissel, M.J., Crick, M., 2001. A cost-benefit analysis of  
524 long-term management options for forests following contamination with <sup>137</sup>Cs. J.  
525 Environ. Radioact. 56, 185–208. [https://doi.org/10.1016/S0265-931X\(01\)00053-4](https://doi.org/10.1016/S0265-931X(01)00053-4)
- 526 Sheppard, S.C., 2005. Transfer parameters-Are on-site data really better? Hum. Ecol. Risk  
527 Assess. <https://doi.org/10.1080/10807030500257747>
- 528 Soukhova, N. V, Fesenko, S. V, Klein, D., Spiridonov, S.I., Sanzharova, N.I., Badot, P.M.,  
529 2003. Cs distribution among annual rings of different tree species contaminated after the  
530 Chernobyl accident, Journal of Environmental Radioactivity.
- 531 Strandgard, M., Walsh, D., 2011. Improving harvester estimates of bark thickness for radiata  
532 pine ( *Pinus radiata* D.Don). South. For. a J. For. Sci. 73, 101–108.

- 533 <https://doi.org/10.2989/20702620.2011.610876>
- 534 Thiessen, K.M., Thorne, M.C., Maul, P.R., Pröhl, G., Wheater, H.S., 1999. Modelling  
535 radionuclide distribution and transport in the environment, in: *Environmental Pollution*.  
536 Elsevier Science Ltd, pp. 151–177. [https://doi.org/10.1016/S0269-7491\(99\)00090-1](https://doi.org/10.1016/S0269-7491(99)00090-1)
- 537 Thiry, Y., Garcia-Sanchez, L., Hurtevent, P., 2015. Experimental quantification of radiocesium  
538 recycling in a coniferous tree after aerial contamination: Field loss dynamics, translocation  
539 and final partitioning. *J. Environ. Radioact.* 161, 42–50.  
540 <https://doi.org/10.1016/j.jenvrad.2015.12.017>
- 541 Thiry, Y., Goor, F., Riesen, T., 2002. The true distribution and accumulation of radiocaesium  
542 in stem of Scots pine (*Pinus sylvestris* L.). *J. Environ. Radioact.* 58, 243–259.  
543 [https://doi.org/10.1016/S0265-931X\(01\)00068-6](https://doi.org/10.1016/S0265-931X(01)00068-6)
- 544 Tyler, A.N., 2008. In situ and airborne gamma-ray spectrometry, in: *Radioactivity in the*  
545 *Environment, Analysis of Environmental Radionuclides*. Elsevier, pp. 407–448.  
546 [https://doi.org/10.1016/S1569-4860\(07\)11013-5](https://doi.org/10.1016/S1569-4860(07)11013-5)
- 547 van der Perk, M., Burema, J., Vandenhove, H., Goor, F., Timofeyev, S., 2004. Spatial  
548 assessment of the economic feasibility of short rotation coppice on radioactively  
549 contaminated land in Belarus, Ukraine, and Russia. I. model description and scenario  
550 analysis. *J. Environ. Manage.* 72, 217–232.  
551 <https://doi.org/10.1016/j.jenvman.2004.05.002>
- 552 Varley, A., Tyler, A., Bondar, Y., Hosseini, A., Zabrotski, V., Dowdall, M., 2018.  
553 Reconstructing the deposition environment and long-term fate of Chernobyl <sup>137</sup>Cs at the  
554 floodplain scale through mobile gamma spectrometry. *Environ. Pollut.* 240, 191–199.  
555 <https://doi.org/10.1016/J.ENVPOL.2018.04.112>
- 556 Varley, Adam, Tyler, A., Dowdall, M., Bondar, Y., Zabrotski, V., 2017. An in situ method for  
557 the high resolution mapping of <sup>137</sup>Cs and estimation of vertical depth penetration in a  
558 highly contaminated environment. *Sci. Total Environ.* 605–606, 957–966.  
559 <https://doi.org/10.1016/j.scitotenv.2017.06.067>
- 560 Varley, A., Tyler, A., Dowdall, M., Bondar, Y., Zabrotski, V., 2017. An in situ method for the

561 high resolution mapping of<sup>137</sup>Cs and estimation of vertical depth penetration in a highly  
562 contaminated environment. Sci. Total Environ. 605–606.  
563 <https://doi.org/10.1016/j.scitotenv.2017.06.067>

564 Vitaly, L., Sokolov, A., Saveliev, A.A., 2019. Spatial analysis and modeling of cesium-137  
565 redistribution in the soil cover of the Bryansk region Spatial analysis and modeling of  
566 cesium-137 redistribution in the soil cover of the Bryansk region, in: EGU General  
567 Assembly 2019At: Viena, Austria.

568 Vitaly, L., Sokolov, A., Saveliev, A.A., Mironenko, I. V, 2018. Landscape-scale modelling to  
569 predict soil lateral migration using Cs-137 on the Bryansk Opolje region ( Russia ) In :  
570 GlobalSoilMap Digital Soil Mapping from Country to Globe Eds . Dom ..., in:  
571 GlobalSoilMap.

572 Woodfuels Program, E., 2009. Program to set up the production of wood pellets (pellets), wood  
573 briquettes and coal in the organizations of the Ministry of Forestry 2009-2011 (in Russian).

574 Yoshihara, T., Matsumura, H., Tsuzaki, M., Wakamatsu, T., Kobayashi, T., Hashida, S. nosuke,  
575 Nagaoka, T., Goto, F., 2014. Changes in radiocesium contamination from fukushima in  
576 foliar parts of 10 common tree species in Japan between 2011 and 2013. J. Environ.  
577 Radioact. 138, 220–226. <https://doi.org/10.1016/j.jenvrad.2014.09.002>

578

579

580

581

582

583

584

585